

FIG. 4. Experimental hyperfine fields vs T/T_C for $\text{Pd}_{1-x}\text{Co}_x$ alloys at 297°K, with pressure the implicit variable. $H_i(p)$ data are the smoothed experimental curves of Fig. 3 and $T_C(p)$ data are taken from Table I. The right-hand ordinate is normalized to $|H_0(p=0)| = 308$ kOe as described in the text. The dashed curve is the molecular-field spontaneous-magnetization function of spin- $\frac{1}{2}$. The arrows indicate the direction of increasing pressure.

relation is easily calculated in the molecular-field approximation and works well if conduction-electron contributions to the impurity moment are small. For a strong response (Fe^{57} in Ni) g lies above f , saturating more quickly as T drops below T_C , while for a weak response (Mn^{55} in Fe) g lies below f and may be sigmoid shaped.^{63,60} Under pressure, then, one must now consider $\zeta(p)$, the pressure dependence of the relative host-impurity magnetic coupling. As before, the hyperfine field follows the magnetization associated with the parent atom as a function of temperature, although the latter quantity is no longer tracking the magnetization of the host. Thus

$$H_i(T) = H_0 g(T/T_C), \quad (4)$$

whence, using Eq. (3), the hyperfine coupling constant is $A = H_i(T)/\mu(T) = H_0/\mu_0$. In this picture, then, the host magnetization $\sigma(T)$ is coupled to the local impurity magnetization $\mu(T)$ via ζ , and $\mu(T)$ is in turn coupled to the impurity hyperfine field $H_i(T)$ via A .

There are thus five phenomenological parameters whose pressure dependence is expected to be of primary importance in interpreting pressure effects on the hyperfine fields associated with well-defined localized-moment impurities in ferromagnetic hosts: T_C , σ_0 , μ_0 , ζ , A . The pressure-dependent quantities most directly related to the observed hyperfine fields are: T_C , $H_0 = A\mu_0$, and ζ . On the other hand, in homogeneous cases the relevant quantities are: T_C and $H_0 = A\sigma_0$, and the parameter ζ does not appear. Information on interactions within the host are given by the pressure (or volume) dependences of T_C and σ_0 ; the pressure dependence of μ_0 , A , and ζ are properties

of the impurity atom itself and of its interaction with the host.

C. Results

We now show, with reference to the parameters outlined above, that it is possible to explain the essential features of the data of Fig. 4 by use of a simple molecular-field picture. Semiquantitative estimates of the pressure dependences of the relevant parameters are obtained. Quantitative determinations, however, will be seen to require further temperature-dependent data which are not currently available. In Fig. 5 we plot a family of impurity response functions $g(T/T_C)$ for impurity spin- $\frac{1}{2}$, parametrized by the relative host-impurity coupling constant ζ , referenced to the host spontaneous-magnetization function $f(T/T_C)$ of spin- $\frac{1}{2}$, all within the molecular-field approximation. $g(T/T_C)$ coincides with $f(T/T_C)$ here when $\zeta = 1.0$. The function $g(T/T_C)$ is related to $f(T/T_C)$ in the molecular-field approximation according to

$$g(T/T_C) = B_{S'} \left(\zeta \frac{f(T/T_C)}{T/T_C} \right), \quad (5)$$

where S' is the impurity spin and $B_{S'}$ is a Brillouin function.^{60,63} The host spontaneous-magnetization function $f(T/T_C)$ need not be expressed within the molecular-field approximation here, but can be the exact experimental function $\sigma(T)/\sigma_0$. Callen *et al.*⁶¹ note that the molecular-field theory is much more accurate for the impurity than for the host,⁶⁵ so Eq. (5) should work well for $g(T/T_C)$ even when the molecular-field theory does not give a good representation of $f(T/T_C)$. [Equation (5) is *exact*, however, only in the weak coupling limit.⁶²] For simple illustrative purposes in Fig. 5 we use the molecular-field theory for f as well as for g (see Appen-

dix).

By considering the functions $g(T/T_C)$ of Fig. 5 to represent possible values of $H_i(T)/H_0$ according to Eqs. (4) and (5), a series of hypothetical pressure-dependent curves can be generated by use of (i) the values $T/T_C(p)$ for each alloy from the data of Table I with $T = \text{const} = 297^\circ\text{K}$ (as was done in Fig. 4) and (ii) an assumed $\zeta(p)$. For example, $\zeta(p) = \text{constant}$ implies that all curves $H_i(T, p)/H_0(p)$ coincide with the same function $g(T/T_C)$ as $T/T_C(p)$ decreases with pressure for each alloy. The dashed segments in Fig. 5 illustrate the effect of a linear decrease of ζ with pressure, from $\zeta = 1.0$ at 0 kbar to $\zeta = 0.6$ at 180 kbar. For purposes of comparison with the data of Fig. 4, however, it is necessary to convert the dashed curves of Fig. 5 to the form $H_i(T, p)$ vs $T/T_C(p)$, i. e., to multiply each dashed segment by $H_0(p)$. The pressure dependence of H_0 is most readily determined for the alloy with lowest T/T_C , since $H_i(T)$ there has greatest sensitivity to changes of H_0 . $H_0(p)$ has thus been "fitted" for Pd_{0.85}Co_{0.15} by requiring that the model curve reproduce the experimental ratio $[H_i(p=180)/H_i(p=0)] = 1.08$ for this alloy (pressure units in kbar), with a linear pressure dependence. The solid segments in Fig. 5 show the effect of applying this same $H_0(p)$ to all four alloys. The right-hand ordinate of Fig. 5 should be compared to the right-hand ordinate of Fig. 4. The similarities to the experimental curves of Fig. 4 are apparent: The $x=0.09$ alloy shows a very dramatic pressure effect; the various $H_i(T, p)$ segments are not continuous, with the $x=0.08$ curve lying below the $x=0.09$ curve and the high-pressure region of the $x=0.12$ curve falling below the low-pressure overlapping T/T_C region of the $x=0.15$ curve; the

over-all increase of $|H_i|$ is greater for the $x=0.12$ alloy than for $x=0.15$ and greater for $x=0.09$ than for $x=0.08$; all curves have qualitatively the correct shapes, increasing most rapidly at the lower pressures and tending to level off at the higher pressures. The values of the two pressure-dependent parameters employed in Fig. 5 are $d \ln \zeta / dp = -2.8 \times 10^{-3} / \text{kbar}$ and $d \ln H_0 / dp = +1.1 \times 10^{-3} / \text{kbar}$, the same for all alloys. The most glaring fault of the model curves of Fig. 5 is the insufficient depression of the $x=0.08$ curve below the $x=0.09$ curve. This difficulty can be rectified somewhat by assuming a larger negative pressure dependence to ζ , and the effect of doing so is shown in Fig. 6, where $\zeta = 0.5$ at 180 kbar and $H_0(p)$ is determined by the same criterion as above. The situation is indeed improved for $x=0.08$ and $x=0.09$ but is worsened for $x=0.12$ and $x=0.15$, because the experimental curves do not show a decrease of $|H_i|$ at the highest pressures. In Fig. 6, $d \ln \zeta / dp = -3.7 \times 10^{-3} / \text{kbar}$ and $d \ln H_0 / dp = +1.7 \times 10^{-3} / \text{kbar}$.

The model curves of Figs. 5 and 6 are not detailed quantitative reproductions of the experimental data for several reasons, although in view of the simplicity of the molecular-field model used and the paucity of pressure-dependent parameters employed the qualitative picture is indeed satisfactory. For example, we have included no variation of the parameters $\zeta(p)$ and $H_0(p)$ with composition, and have moreover assumed linear pressure dependences for these quantities. The major obstacle to a more quantitative analysis of the present pressure-dependent data, however, lies in the lack of a satisfactory $p=0$ "baseline" for each alloy from which a realistic set of the ζ -dependent functions $g(T/T_C)$ can be obtained from Eq. (5) or from

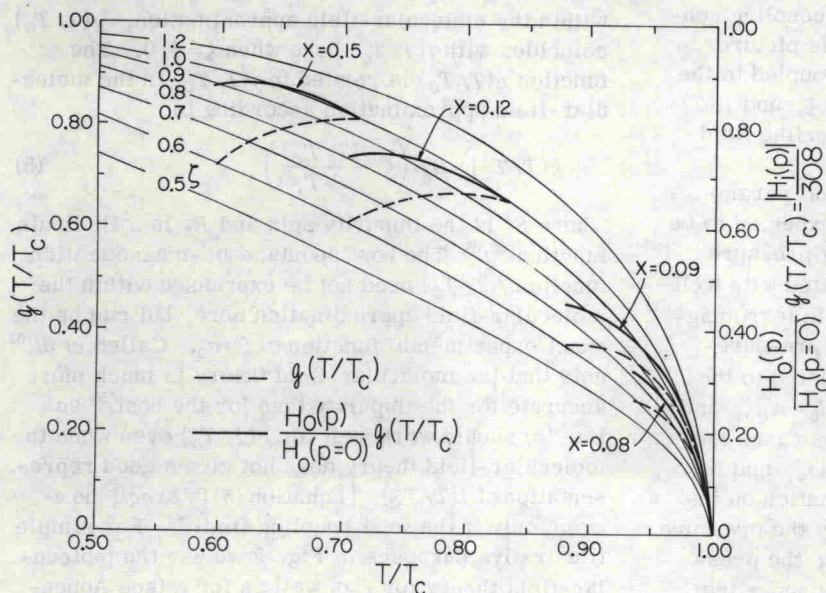


FIG. 5. Model curves of normalized hyperfine fields vs T/T_C . Light lines: molecular-field impurity response functions, parametrized by ζ as described in the text. Dashed lines: hypothetical pressure-dependent impurity response curves using $T_C(p)$ from Table I and $\zeta(p)$ as described in the text. Heavy lines: dashed lines modified by pressure-dependent $H_0(p)$ as described in the text, representing normalized hyperfine field curves to be compared to the right-hand ordinate of Fig. 4.